

Integrated three-dimensional microelectromechanical devices from processable carbon nanotube wafers

YUHEI HAYAMIZU¹, TAKEO YAMADA¹, KOHEI MIZUNO¹, ROBERT C. DAVIS², DON N. FUTABA¹,
MOTOO YUMURA¹ AND KENJI HATA^{1*}

¹Nanotube Research Center, National Institute of Advanced Industrial Science and Technology (AIST), Tsukuba 305-8565, Japan

²Department of Physics and Astronomy, Brigham Young University, Provo, Utah 84602, USA

*e-mail: kenji-hata@aist.go.jp

Published online: 4 May 2008; doi:10.1038/nnano.2008.98

In order to be useful as microelectromechanical devices, carbon nanotubes with well-controlled properties and orientations should be made at high density and be placed at predefined locations. We address this challenge by hierarchically assembling carbon nanotubes into closely packed and highly aligned three-dimensional wafer films from which a wide range of complex and three-dimensional nanotube structures were lithographically fabricated. These include carbon nanotube islands on substrates, suspended sheets and beams, and three-dimensional cantilevers, all of which exist as single cohesive units with useful mechanical and electrical properties. Every fabrication step is both parallel and scalable, which makes it easy to further integrate these structures into functional three-dimensional nanodevice systems. Our approach opens up new ways to make economical and scalable devices with unprecedented structural complexity and functionality.

Owing to their fascinating physical and chemical properties, the use of carbon nanotubes (CNTs) has been extensively pursued in nanodevices such as microelectromechanical systems (MEMS), although efforts to date have primarily focused on demonstrations of individual CNTs and single nanodevices. For example, a suspended nanotube has been used as a device element of tuneable electromechanical oscillators¹, sensors^{2,3}, non-volatile memory⁴, rotational actuators⁵ and even a nanotube radio⁶. Similarly, a carbon nanotube cantilever has been used for a scanning probe microscope tip⁷, nanotweezers⁸, switches^{9,10} and relays¹¹. An alternative and perhaps more realistic approach to realizing reliable and integrated nanodevice systems is to assemble a predetermined massive quantity of CNTs at prescribed locations and shape them into well-defined and controlled configurations. With this approach, individual nanodevices would be made from a number of nanotubes, thus opening up an exciting opportunity to design versatile and rational nanodevices with higher-level structural diversity and complexity. Bottom-up self-assembly has emerged as a new paradigm to assemble nanotubes. The successful self-assembly of carbon nanotubes into aligned networks or multilayer systems has been reported using Langmuir–Blodgett techniques¹² and substrate oriented growth¹³. Although each represents valuable advances, particularly in the area of field-effect transistors, the density, complexity and control of the assembly is insufficient to realize functional and integrated CNT MEMS. This paper presents a scalable and reliable bottom-up and top-down hybrid methodology where individual nanotubes are hierarchically assembled by two self-assembly stages into closely packed and aligned nanotubes films that we denote as ‘CNT wafers.’ Our

architecture allows the realization of diverse, well-defined, and complex CNT device elements as single cohesive units that possess the mechanical and electrical properties that enable them to serve as building-blocks for integrated device systems.

ASSEMBLY AND PROCESSING OF CNT WAFERS

Figure 1a illustrates the steps of the hierarchical assembly scheme. Two hierarchical bottom-up self-assembly stages guide nanotubes into a highly densely packed nanotube solid-film form that we term a CNT wafer. First, highly efficient growth self-assembles single-walled carbon nanotubes (SWNTs) into vertically aligned sparse forest films¹⁴. Second, a liquid induced zippering effect self-assembles the sparse SWNTs into a CNT wafer. Conventional top-down lithography then processes the wafer into nanodevice systems. In some sense, the SWNT-to-CNT wafer assembly is analogous to the self-assembly of silicon atoms to silicon wafers by epitaxial growth; moreover, there are similarities between how silicon devices are etched from silicon wafers and how CNT devices are cut from CNT wafers. More uniquely, the flexibility of nanotubes enables three-dimensional (3D) wafers to be built, from which we can design and etch out rational 3D devices that would be difficult to make using other materials and methods.

Specifically, a regular array of vertically aligned SWNT forest films of a few hundred micrometres in height (Fig. 1b) were first synthesized by water-assisted chemical vapour deposition (CVD), a process known as ‘super-growth’¹⁴. Structural characterization of the forest can be found in the literature¹⁵. Briefly, the SWNTs in the forests have an average diameter of 2.8 nm, are very long, aligned and catalyst-free, with a carbon purity of >99.9%¹⁴.

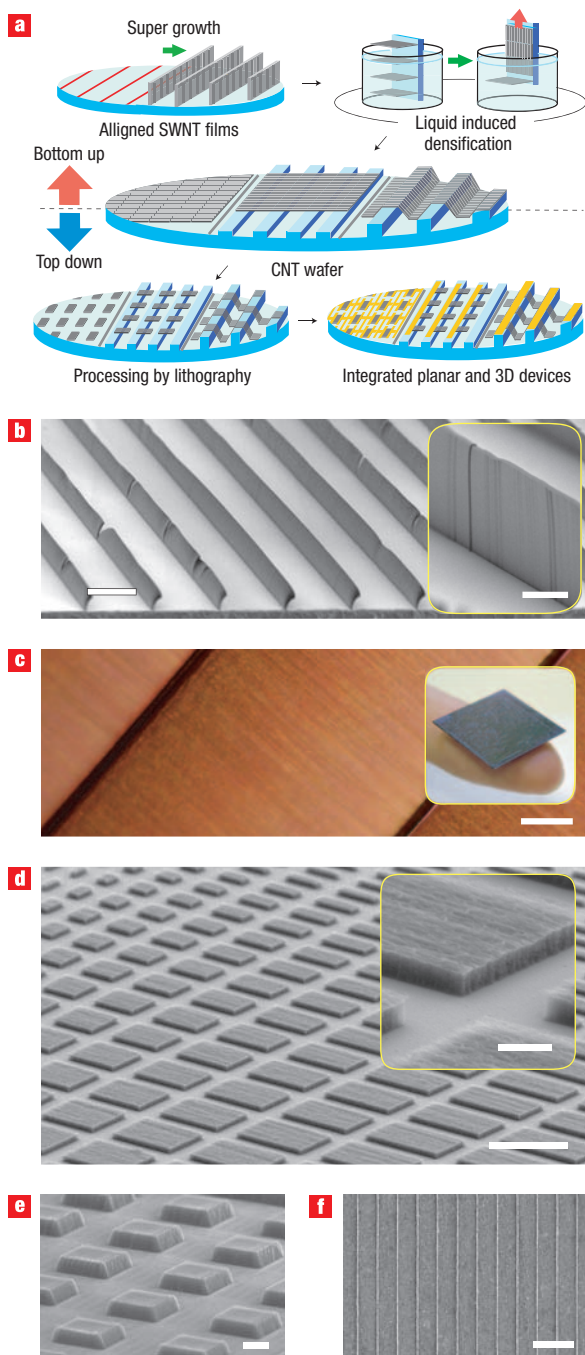


Figure 1 Schematic illustration and fabrication of planar/3D CNT wafers and islands. **a**, An array of vertically aligned SWNT forests were synthesized, densified into a CNT wafer by alcohol solution, and processed by lithography into arbitrary shapes. **b**, SEM image of an array of vertically aligned forest films. Scale bar, 200 μm . Inset: enlarged SEM image. Scale bar, 50 μm . **c**, Optical microscope image of a CNT wafer. Scale bar, 100 μm . Inset: image of a 2 cm \times 2 cm CNT wafer. **d**, SWNT planar islands having a diverse range of sizes. Scale bar, 5 μm . Inset: enlarged SEM image. Scale bar, 1 μm . **e**, SEM image of parallelepipeds. Scale bar, 100 μm . **f**, SEM image of SWNT beams of 40 nm width and 70 nm height. Scale bar, 2 μm .

The alignment of the nanotubes within a forest is imperfect¹⁴, and thus nanotubes form small bundles that enable vertical orientation¹⁶. The forest is a very sparse material and nanotubes only occupy 3–4% of the total volume (nanotube

density, 4×10^{11} tubes cm^{-2}). This forest sparseness translates to film flexibility, which enables diverse multidimensional designs.

The substrate with forest films was drawn through an isopropyl alcohol (IPA) solution to horizontally redirect the vertical alignment (Fig. 1a,c) and dried using nitrogen gas. When liquids were introduced into the sparse SWNT forest and dried, the surface tension of the liquids and the strong van der Waals interactions effectively ‘zip’ the SWNTs together to near-ideal graphitic spacing. This self-assembly transformed a sparse forest film into a highly densely packed form of homogeneous SWNT bulk material; we have denoted this a ‘CNT wafer’ because of its behaviour as a continuous medium (see Supplementary Information, Fig. S1). Typically, forest densification occurred in the two lateral directions¹⁷; however, substrate–forest interaction and lateral SWNT orientation guided densification in only one direction to essentially ‘flatten’ the forest to the substrate with strong adhesion. Once densified, the SWNTs did not disassemble, and the wafer could then be treated as a single body. In contrast to making films using material deposition, where achievable film thicknesses are limited by a finite deposition rate and unacceptable stress accumulation, we could fabricate CNT wafers covering a wide range of thicknesses (100 nm–100 μm) with the same process by using forests of different thicknesses.

These self-assembly processes are fundamentally scalable. The size of individual films is limited by the current status of synthesis technology, but the CNT wafer size can be increased by synthesizing a film array. The height of the films can be grown to match the pitch between catalyst islands by controlling the growth time. In addition, when flattened and densified, the forests did not shrink in the aligned direction, and thus a CNT wafer made from a film array could encompass large areas of the substrate with fair homogeneity, as we have demonstrated with a 2 cm \times 2 cm CNT wafer (Fig. 1c and inset). These large-scale CNT wafers can serve as templates to integrate numerous nanotube structures and devices. Currently, the discontinuities between adjacent forest films limit the size of the system; however, accounting for the recent progress in CVD in growing films with heights up to 1 cm (7 mm)¹⁸, we envision in the near future the possibility of growing large films that cover the entire die with discontinuities between films located at the cutting edge.

Importantly, lithographic resists could be uniformly coated on the CNT wafers because of the cohesiveness and flatness of the CNT surface, and adhesion with the substrate was sufficient to withstand lithographic processes including heat treatment, immersion into liquids and critical point drying. Using a resist as a mask, the CNT wafers could be etched vertically with a high aspect ratio by oxygen/argon reactive ion etching. Standard lithography could pattern the wafer into arbitrarily shaped SWNT islands in desired positions as demonstrated by the array of islands having diverse sizes shown in Fig. 1d (see also Supplementary Information, Fig. S2). Two additional fabrication examples (Fig. 1e,f) highlight the wide range of material that can be assembled using our approach, from the macroscopic bulk level down to a single nanotube bundle level. At the macroscopic level we fabricated SWNT parallelepipeds consisting of 1.0×10^9 nanotubes from a 100- μm -thick CNT wafer, and at the nanoscopic level we made SWNT beams of 40 nm width (resolution of the electron-beam lithography, EBL) and 70 nm height consisting of ~ 200 SWNTs that resemble nanotube bundles.

STRUCTURAL AND ELECTRICAL PROPERTIES OF CNT WAFERS

Structural and electrical properties of CNT wafers were studied in a series of experiments. Transmission electron microscopy (TEM) of a very thin CNT wafer (250 nm) showed that the nanotubes

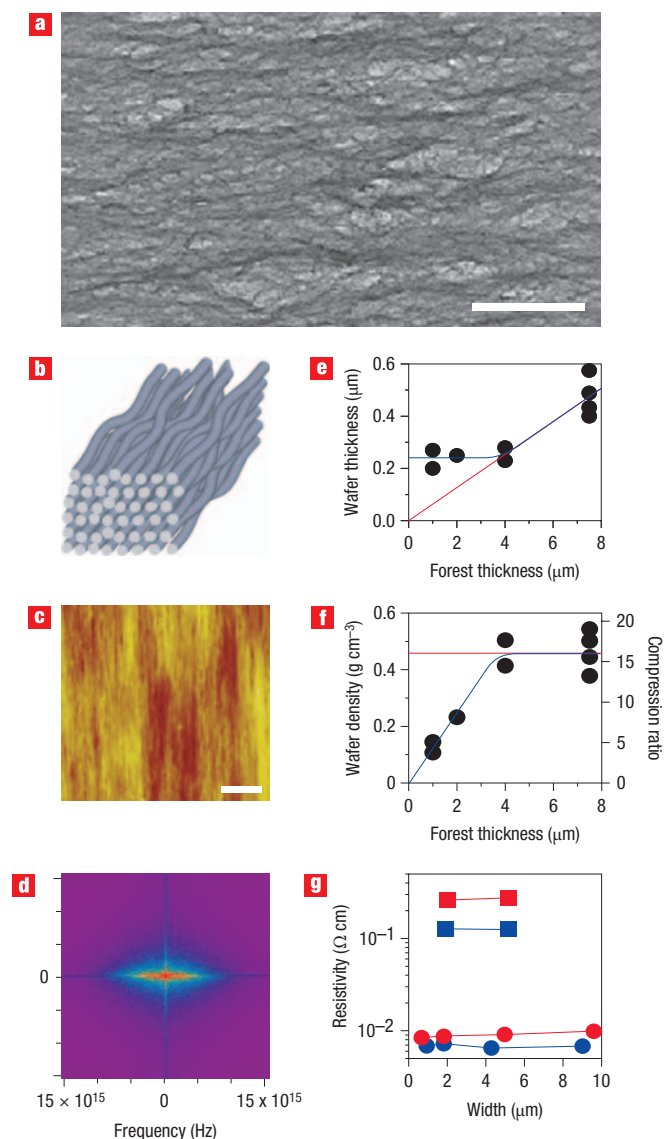


Figure 2 CNT wafer characterization. **a**, TEM image of a 250-nm-thick CNT wafer showing the packing of SWNTs, imperfect alignment, and the absence of voids. **b**, Illustration of tube alignment showing the importance of imperfect alignment on lateral interconnection. **c, d**, AFM image of the CNT wafer surface (**c**, scale bar, 1 μm) and corresponding fast-Fourier transform (**d**). **e, f**, Dependence of CNT wafer thickness (**e**) and density (**f**) on the initial forest film thickness. Red lines represent extrapolation of the dependencies from the thick forest region. **g**, Resistivity of the CNT wafer as a function of wafer width for 306-nm- and 835-nm-thick wafers (red and blue symbols, respectively) and measurements parallel (circles) and perpendicular (squares) to the alignment axis.

within the CNT wafer were closely packed without any voids, and were not perfectly aligned (Fig. 2a). This imperfection provided the essential lateral interconnection for mechanical cohesiveness (Fig. 2b). The degree of alignment (Herman's orientation factor) was calculated to be 0.57 from the intensity profile (Fig. 2c) of the fast-Fourier transform of an atomic force microscopy (AFM) image of the CNT wafer (Fig. 2d; see also Supplementary Information, Fig. S3). This corresponds to an ideally aligned sample being offset from the alignment direction

by 33° . Examination of the relationship between the CNT wafer thickness and density with forest thickness revealed that the wafer thickness did not increase for forest thicknesses below 4 μm (Fig. 2e) but the density did increase monotonically (Fig. 2f). Above this value, the wafer thickness increased monotonically and the density stayed constant at 0.46 g cm^{-3} with increasing forest thickness. The CNT wafer density (0.46 g cm^{-3}) from forests thicker than 4 μm matched well with the density of a macroscopic bulk form of densified forest¹⁷, and corresponded to a SWNT volume occupancy of 42% and tube-to-tube spacing of 1.3 nm. This represents a 58% ideal packing when compared with ideally packed 2.8-nm SWNTs with graphitic spacing of 0.34 nm. These analyses and experimental data showed the CNT wafer to be a solid cohesive single unit. The four-probe resistivity of the CNT wafer with different widths (0.7–9.6 μm) and thicknesses (306 and 835 nm) was established to be 0.008 and $0.2 \Omega \text{ cm}$, parallel and perpendicular to the alignment, respectively (Fig. 2g; see also Supplementary Information, Fig. S4).

FROM CNT WAFER TO MULTIDIMENSIONAL CNT STRUCTURES

We extended this basic planar approach to suspended wafers and structures. CNT wafers were created over prefabricated silicon trenches and pillars (Fig. 3a,b). Although the SWNT forest films were very sparse and thin, the resultant CNT wafers behaved like the skin of a drum without wrinkles or tears (Fig. 3b). Significantly, despite the small contact area between the wafer and the substrate, and the voids between the nanotubes and the substrate, the suspended sparse forest could be flattened and densified by liquids into a suspended CNT wafer while retaining its original shape (Fig. 3b). Although suspended, the wafer could be lithographically processed into arbitrary shapes, demonstrated by the suspended sheets and beams interconnecting silicon pillars (Fig. 3c; see also Supplementary Information, Fig. S5). Notably, we could fabricate suspended beams both parallel and perpendicular to the nanotube alignment, highlighting the structural diversity possible. A suspended beam consists of 20,000 times more nanotubes than achieved in previous studies, where an average number of ~ 1 nanotube was suspended during growth¹⁹. Additional fabrication complexity was illustrated by lithographically etching the suspended wafer between trenches to create a series of cantilevers (Fig. 3d,e; see also Supplementary Information, Fig. S6) with varying configurations. Although thousands of SWNTs were assembled across the tops of the pillars, no trace of SWNTs was detected by Raman spectroscopy on the lower substrate surface, which was important for electrical isolation. These suspended structures could serve as key elements for various CNT nanodevice systems, including electromechanical oscillators¹, nonvolatile memory⁴ and rotational actuators⁵.

The potential to fabricate 3D CNT wafers and structures was also explored using multi-tier substrates and removable support layers ('sacrificial layers'). Nanotube flexibility and strength allowed the forest films to be laid onto multi-tier substrates and transformed into 3D CNT wafers (Fig. 3f) while retaining their original form, and lithographically processed into multi-tier interconnects (Fig. 3g; see also Supplementary Information, Fig. S7). This concept was further extended by using SiO_2 sacrificial layers. Three-dimensional CNT wafers were prepared on SiO_2 templates and processed by lithography (Fig. 3h). By removing the sacrificial layer using hydrofluoric acid, a predefined supported area could be released, and then suspended by a 3D support with designed structures, demonstrated here

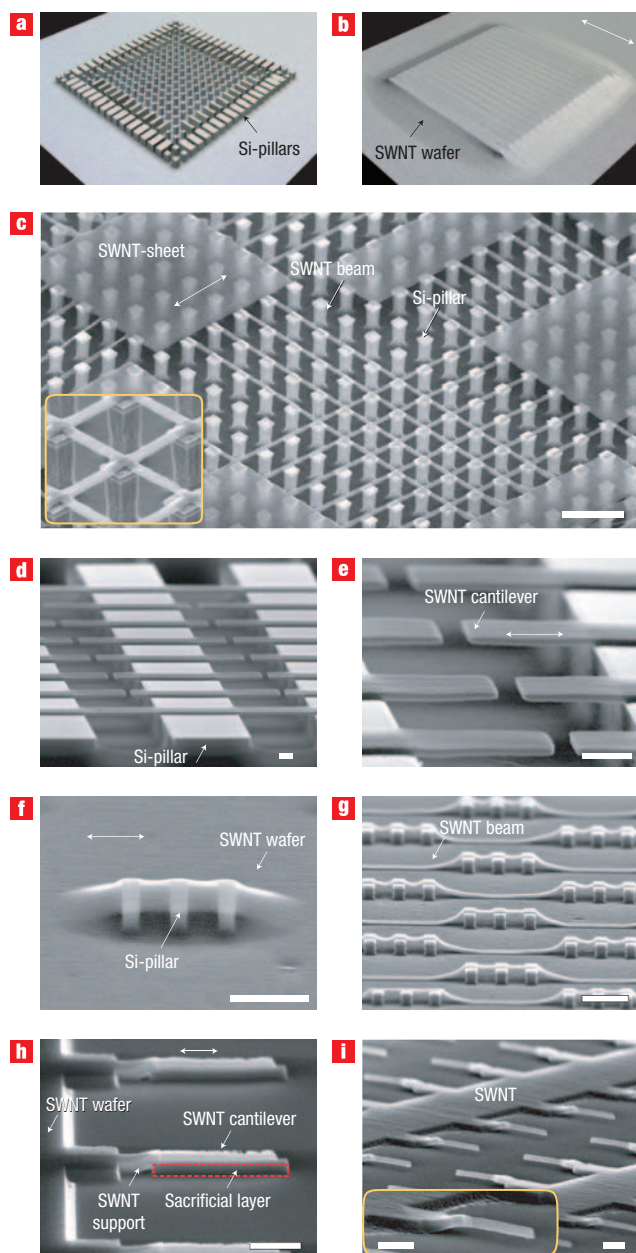


Figure 3 Nonplanar and multitier 3D CNT wafers and structures. **a,b**, Angled view confocal scanning laser micrographs of a set of silicon pillars (**a**, height, 5 μm ; area, 2 $\mu\text{m} \times 2 \mu\text{m}$; pitch 4 μm) and a CNT wafer (**b**, thickness, 250 nm) assembled on top of the pillars. **c**, SEM image of suspended SWNT sheets and beams (width, 1 μm) on silicon pillars. Scale bar, 10 μm . Inset: enlarged SEM image of a beam-crossing. Scale bar, 1 μm . **d,e**, SEM images of cantilevers (width, 5 μm) with lengths varying from 2 to 7 μm on silicon trenches (width, 10 μm ; 10- μm intervals). Scale bar, 2 μm . **f,g**, SEM images of a 3D multitier CNT wafer and multitier interconnects. Scale bar, 10 μm . **h,i**, SEM images of 3D SWNT cantilevers (width, 200 nm; thickness, 500 nm; length, 4 μm) with the sacrificial 440-nm SiO_2 layer (red box) underneath (**h**), and suspended without the sacrificial layers (**i**). The cantilever is seamlessly connected by a SWNT 3D support to the CNT wafer. Scale bar, 2 μm . Inset to **i**: Enlarged SEM image of a cantilever. Arrows indicate the direction of SWNT alignment.

with an array of CNT cantilevers (Fig. 3i; see also Supplementary Information, Fig. S8) with a width of 200 nm. This capability to fabricate 3D structures from nonplanar wafers opens up a new

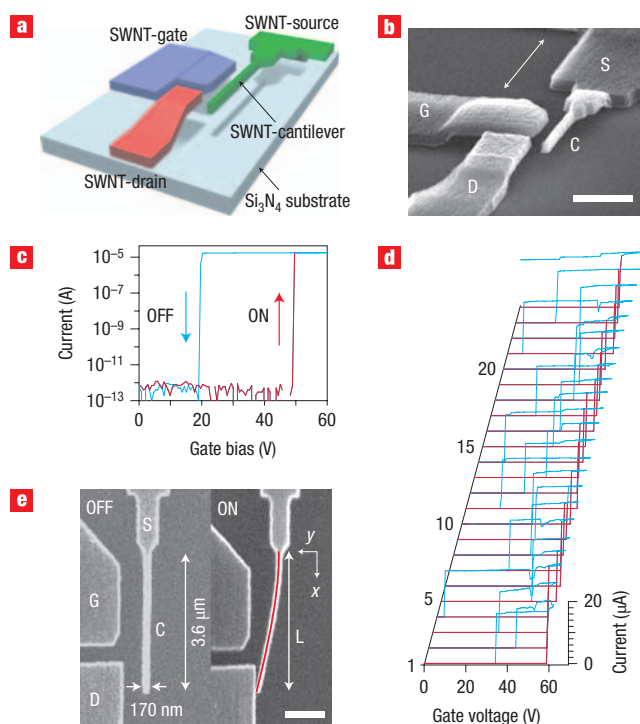


Figure 4 An all-SWNT 3D relay. C, S, D, and G refer to the cantilever and, source, drain and gate electrodes, respectively. **a,b**, Device schematic (**a**) and SEM image (**b**) showing the 3D structure of the CNT relay. SWNT cantilevers (length, 3.6 μm ; width, 170 nm; thickness, 500 nm) were suspended 440 nm from the substrate. SWNT gate and drain electrodes were partially suspended on the same plane with distances of 650 nm and 550 nm from the cantilever, respectively. Scale bar, 2 μm . **c**, Source–drain current versus gate voltage. The relay switched ON/OFF when the gate voltage was ramped up/down (red/blue lines). **d**, Source–drain current versus gate voltage curves showing 23 ON/OFF switching cycles. Finally, the device failed to switch OFF. **e**, Top-view SEM images of OFF (left) and ON (right) cantilevers. The red line describes predicted bending of a continuous cantilever under point loading at the free end. Scale bar, 1 μm .

frontier in designing rational 3D devices that are impossible to fabricate using bulk micromachining.

FABRICATION OF OPERATIONAL CNT RELAYS

These techniques can be integrated to fabricate nanodevices with a determined functionality based on structural design. The potential of our approach was probed for a CNT relay. Although a CNT relay is desirable as a high-speed switching element²⁰, the fabrication of operationally reliable CNT relays is challenging, because it requires the gate–cantilever electrostatic attractive force to overcome the cantilever restoring force for pull-in (ON), yet the restoring force must be sufficiently strong to overcome the cantilever–drain sticking force for pull-off (OFF). To meet these requirements, we fabricated a CNT relay (Fig. 4a,b; see also Supplementary Information, Fig. S9) composed of a 170-nm-wide cantilever connected to a 3D electrode associated with two 3D nanotube source and gate electrodes arranged in predefined locations. All device components were made from the same SWNT film and were carefully designed in configuration and fabricated with high precision to achieve operational devices. Because a 10-nm error in cantilever width would result in a 16%

change in the restoring force, fabrication precision was critical. The use of sacrificial layers was indispensable for precise coplanar positioning of the CNT cantilever and electrodes, the stepwise widening of the cantilever connection, and 3D crank shapes of the drain and source electrodes. The device designs including the 3D configuration of the cantilever and position of the electrodes were further optimized to balance the cantilever restoring force and electrostatic interaction between electrodes. For example, the gate electrode was positioned to maximize electrostatic interaction with the cantilever while avoiding direct contact.

These structural architectures were assessed for electromechanical switching of the cantilever between well-defined ON and OFF states controlled by the gate electrode (Fig. 4c). The gate bias was cyclically swept between 0 and 60 V, and 5 V was applied between the source and drain with a 250 k Ω load resistance. At zero gate voltage, the cantilever was OFF and no source–drain current flowed. At the ON gate voltage, the cantilever was instantaneously pulled in, creating the ON state, and the source–drain current increased over 10^7 times while the gate remained electrically isolated. Currents well beyond 100 μ A (270 μ W) could be passed. Decreasing the gate voltage allowed the mechanical restoring force of the cantilever to return the relay to the OFF state. The cantilever moved as a single body despite being composed of $\sim 5,000$ SWNTs. The well-defined and reversible electrical and mechanical ON and OFF states, and the very high ON/OFF current ratio have not been reported in previous studies of individual nanotube CNT relays¹¹.

Variations in the OFF voltages (Fig. 4d) arose from the cantilever–drain sticking force (that is, van der Waals forces or the adhesive force of water), which limited the long-term device performance. Application of 23 repeated ON/OFF cycling of an individual CNT relay shows the variation in the OFF voltages from consecutive cycles, although the ON voltage remained fairly consistent before failure. The relatively large ON voltage was designed to meet the requirement for reversible switching; without this it could have been reduced to 1.5 V. The maximum duration time of the ON state was 2.0 s. To date, because of limitations arising from the sticking force, the optimum batch yield we have achieved for reversible switching is 63% (the yield for irreversible switching was above 90%). Substantial improvement in performance should be possible by vacuum operation or by redesigning the contact area.

Mechanical properties of the cantilever were derived from the electromechanical characteristics. We found that the cantilever deflection in the ON state fitted well with the deflection of a continuous cantilever under point loading at the free end (Fig. 4e). The fine match indicated that the cantilever acted as a single elastic body that could be described by classical mechanics. Under the assumption that the cantilever and the gate electrode were two parallel plates, the spring constant and modulus of the rectangular cantilever were estimated to the first order as $k = 0.38 \text{ N m}^{-1}$ and $E = 9.7 \text{ GPa}$, respectively, using the ON voltage and cantilever dimensions. Considering the actual configuration of the gate electrode and cantilever, the modulus of the cantilever was underestimated. The estimated Young's modulus is superior to most CNT ropes and fibres (for example, the modulus of yarned nanotube fibers is between 150 MPa and $\sim 460 \text{ MPa}$)²¹, yet much lower than the $\sim 1 \text{ TPa}$ modulus^{22,23} of individual CNTs because intertube slippage degrades the mechanical property. Finally, the resonance frequency was calculated as $f = 13.7 \text{ MHz}$. The resonance frequency was similar to that calculated for a silicon cantilever with the same configuration (19.2 MHz). We believe that it is significant that CNT-MEMS possessing a comparable resonance

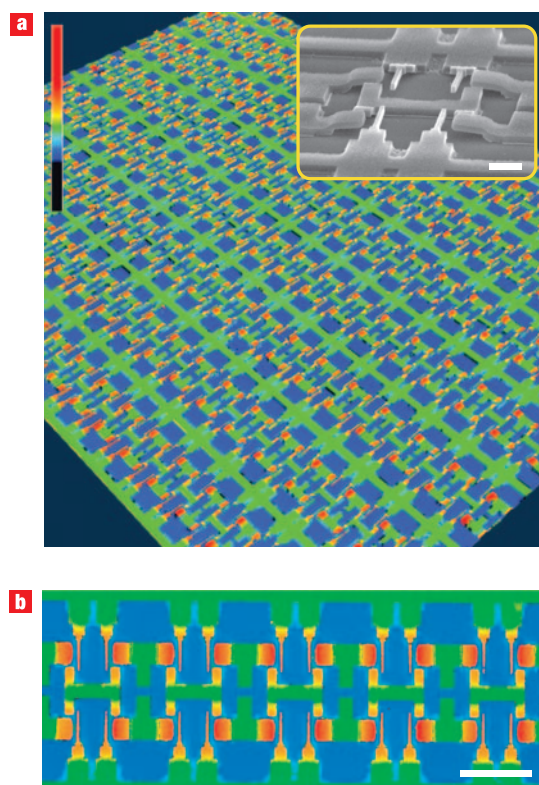


Figure 5 Parallel fabrication of 1,276 CNT relays. **a,b**, 3D height images collected by confocal scanning laser microscopy on an array of 1,276 3D SWNT relays with the same configurations as Fig. 4, but with no individual electric addresses to each electrode: angled view (**a**); top view (**b**). Scale bar, 10 μm . Inset: SEM image showing the 3D structure. Scale bar, 2 μm . The device size is $6.8 \mu\text{m} \times 10 \mu\text{m}$, and the size of the device array is $410 \mu\text{m} \times 310 \mu\text{m}$.

frequency as bulk micromachined silicon-MEMS can be achieved by this surface micromachining approach, because the unique SWNT properties, such as high surface area, can be incorporated into advanced nanodevices not possible from silicon in bio- and chemical sensors.

PARALLEL PROCESSING OF COMPLEX CNT STRUCTURES

Each fabrication stage of our approach is intrinsically highly parallel and scalable. To demonstrate the scalability potential of our approach, 1,276 identical integrated CNT nanodevices as described above were fabricated in parallel (see Supplementary Information, Fig. S10). The 3D bird's-eye-view height maps (Fig. 5) of the device array demonstrate that these devices have well-defined and identical 3D structures, and the structural yield was estimated as 95.5%. Reproducible and controlled parallel device fabrication is one of the most crucial goals for nanomaterials to be integrated into real systems and has been demonstrated here by the excellent uniformity, scalability and controllability of the highly efficient nanotube growth and liquid induced guided self-assembly.

Thus, we have shown a general approach to assembling SWNTs into a highly densely packed form of homogeneous SWNTs films—CNT wafers—from which functional and integrated nanodevice systems may be fabricated by lithography. Our initial efforts focused on demonstrating diverse 3D structures, and the promise of these new structures was highlighted by demonstrating a 3D

CNT relay. We believe that future advancement of this approach could revolutionize CNT-MEMS devices, as previously demonstrated on individual nanotubes.

METHODS

GROWTH OF VERTICALLY ALIGNED SWNT FOREST FILMS

Vertically aligned SWNT forest films a few hundred micrometres in height (Fig. 1b) were synthesized by water-assisted CVD¹⁴ from catalyst lines patterned using EBL (EB machine, CABL8000, Crestec) on a silicon substrate (100-nm oxide layer) at 750 °C for 3–10 min. The catalysts were patterned by the following process. First, 350-nm-thick EB-resist (ZEP-520A, Zeon) was exposed by EB and developed by ZED-N50 (Zeon). Second, a catalyst thin film of Al₂O₃ (10 nm)/Fe (1 nm) was sputtered, and the resist mask was lifted off using a remover (ZDMAC, Zeon). The size of the patterned catalyst and the growth time of CVD determined the thickness and the height of the films, respectively. The high catalyst activity of 84% allowed for nanotube self-assembly into vertically aligned, homogeneous forest-film structures¹⁵.

SWNT PLANAR ISLANDS

To make SWNT planar islands (Fig. 1d), a SWNT film (height, 500 µm; width, 1 mm; thickness, 4 µm) was laid on a 100-nm-thick nickel-coated Si₃N₄ substrate (200-nm-thick Si₃N₄ layer on a silicon substrate) and transformed into a CNT wafer by IPA solution. Then, 440-nm hydrogen silsesquioxane (HSQ) (FOX16, Dowcorning) was spin-coated and baked at 90 °C for 10 min. HSQ was then patterned using EBL and developed by tetramethylammoniumhydroxide (TMAH) solution (2.38%, ZTMA-100, Zeon). The CNT wafer with HSQ mask was etched by reactive ion etching (RIE) (RIE-200L, Samco) with oxygen and argon (80 W, 10 Pa, 10 s.c.c.m. oxygen, 1 min; 80 W, 10 Pa, 10 s.c.c.m. oxygen, 10 s.c.c.m. argon, 2 min). The HSQ mask was removed by buffered hydrofluoric acid (HF) (4.7% HF, 36.2% NH₄F, 59.1% H₂O, Morita Chemical Industries), and the sample was dried by means of critical point drying with CO₂ (critical point dryer, SCD4, Ryusyo Industrial).

SUSPENDED SWNT SHEETS, BEAMS, CANTILEVERS AND 3D MULTI-TIER INTERCONNECTS

Silicon pillars and trenches were fabricated from a silicon substrate (500-nm-thick oxide layer) with a 100-nm-thick nickel mask etched by RIE (100 W, 8.5 Pa, 40 s.c.c.m. CHF₃, 60 s.c.c.m. SF₆, 55 s.c.c.m. oxygen). A CNT forest with a thickness of 4 µm was placed across these silicon pillars and transformed into a CNT wafer using IPA solution. Then, 440 nm HSQ (FOX16, Dowcorning) was spin-coated and baked at 90 °C for 10 min. HSQ was patterned using EBL and developed by TMAH solution (2.38%, ZTMA-100, Zeon). The CNT wafer with the HSQ mask was etched by RIE (RIE-200L, Samco) with oxygen and argon (80 W, 10 Pa, 10 s.c.c.m. oxygen, 1 min; 80 W, 10 Pa, 10 s.c.c.m. oxygen, 10 s.c.c.m. argon, 2 min). The HSQ mask was removed by buffered HF (4.7% HF, 36.2% NH₄F, 59.1% H₂O, Morita Chemical Industries) and the sample was dried in air. In the case of 3D multitier interconnects, the HSQ mask was removed by HF vapour from 50% HF solution.

3D CANTILEVER AND CNT RELAY

As a sacrificial layer, HSQ with a thickness of 440 nm was spin-coated on a Si₃N₄ substrate (200-nm-thick Si₃N₄ layer on silicon substrate). After soft-baking (250 °C, 2 min), the HSQ was patterned and converted to SiO₂ by EBL exposure and developed by TMAH solution (2.38%, ZTMA-100, Zeon). The CNT wafer was made and patterned into 3D SWNT cantilevers and electrodes on this substrate by the same process as SWNT planar islands.

DEFLECTION OF THE CNT CANTILEVER

Bending of a continuous cantilever under point loading at its free end is described by $y(x) = (F/6EI)(3Lx^2 - x^3)$, where the x and y coordinates are shown in Fig. 4e, F is the force, E is Young's modulus, I is the moment of inertia, and L is length²⁴.

CALCULATIONS OF YOUNG'S MODULUS AND RESONANCE FREQUENCY OF CNT CANTILEVERS

Under the assumption that the cantilever and the gate electrode behaved as two parallel plates, the spring constant and modulus of the rectangular cantilever were estimated using the ON voltage and cantilever dimensions from $k = (27CV_p^2/8g^2)$ and $E = (27CV_p^2L^3/2g^2tw^3)$, where C is the capacitance, g is the gate-cantilever gap, V_p is the ON voltage, and t , L and w are the thickness, length and width of the cantilever, respectively. The resonance frequency was calculated as $f = 13.7$ MHz from $f = 0.162(w/L^2)\sqrt{(E/\rho)}$, where ρ [0.232(g cm⁻³)] is the density²⁵.

Received 9 January 2008; accepted 1 April 2008; published 4 May 2008.

References

- Sazonova, V. *et al.* A tunable carbon nanotube electromechanical oscillator. *Nature* **431**, 284–287 (2004).
- Kong, J. *et al.* Nanotube molecular wires as chemical sensors. *Science* **287**, 622–625 (2000).
- Stampfer, C. *et al.* Fabrication of single-walled carbon-nanotube-based pressure sensors. *Nano Lett.* **6**, 233–237 (2006).
- Rueckes, T. *et al.* Carbon nanotube-based nonvolatile random access memory for molecular computing. *Science* **289**, 94–97 (2000).
- Fennimore, A. M. *et al.* Rotational actuators based on carbon nanotubes. *Nature* **424**, 408–410 (2003).
- Jensen, K., Weldon, J., Garcia, H. & Zettl, A. Nanotube radio. *Nano Lett.* **7**, 3508–3511 (2007).
- Dai, H., Hafner, J. H., Rinzler, A. G., Colbert, D. T. & Smalley, R. E. Nanotubes as nanoprobe in scanning probe microscopy. *Nature* **384**, 147–150 (1996).
- Kim, P. & Lieber, C. M. Nanotube nanotweezers. *Science* **286**, 2148–2150 (1999).
- Deshpande, V. V. *et al.* Carbon nanotube linear bearing nanoswitches. *Nano Lett.* **6**, 1092–1095 (2006).
- Jang, J. E. *et al.* Nanoscale memory cell based on a nanoelectromechanical switched capacitor. *Nature Nanotech.* **3**, 26–30 (2008).
- Lee, S. W. *et al.* A three-terminal carbon nanorelay. *Nano Lett.* **4**, 2027–2030 (2004).
- Li, X. *et al.* Langmuir–Blodgett assembly of densely aligned single-walled carbon nanotubes from bulk materials. *J. Am. Chem. Soc.* **129**, 4890–4891 (2007).
- Kang, S. J. *et al.* High-performance electronics using dense, perfectly aligned arrays of single-walled carbon nanotubes. *Nature Nanotech.* **2**, 230–236 (2007).
- Hata, K. *et al.* Water-assisted highly efficient synthesis of impurity-free single-walled carbon nanotubes. *Science* **306**, 1362–1364 (2004).
- Futaba, D. N. *et al.* 84% catalyst activity of water assisted growth of single walled carbon nanotube forest characterization by a statistical and macroscopic approach. *J. Phys. Chem. B* **110**, 8035–8038 (2006).
- Einarsson, E. *et al.* Revealing the small-bundle internal structure of vertically aligned single-walled carbon nanotube films. *J. Phys. Chem. C* **111**, 17861–17864 (2007).
- Futaba, D. N. *et al.* Shape-engineerable and highly densely packed single-walled carbon nanotubes and their application as super-capacitor electrodes. *Nature Mater.* **5**, 987–994 (2006).
- Chakrabarti, S., Nagasaki, T., Yoshikawa, Y., Pan, L. & Nakayama, Y. Growth of super long aligned brush-like carbon nanotubes. *Jpn J. Appl. Phys.* **45**, L720–L722 (2006).
- Homma, Y., Kobayashi, Y., Ogino, T. & Yamashita, T. Growth of suspended carbon nanotube networks on 100-nm-scale silicon pillars. *Appl. Phys. Lett.* **81**, 2261–2263 (2002).
- Kinaret, J. M., Nord, T. & Viefers, S. A carbon-nanotube-based nanorelay. *Appl. Phys. Lett.* **82**, 1287–1289 (2003).
- Zhang, M., Atkinson, K. R. & Baughman, R. H. Multifunctional carbon nanotube yarns by downsizing an ancient technology. *Science* **306**, 1358–1361 (2004).
- Yu, M. F. *et al.* Strength and breaking mechanism of multiwalled carbon nanotubes under tensile load. *Science* **287**, 637–640 (2000).
- Khang, D. Y. *et al.* Molecular scale buckling mechanics in individual aligned single-wall carbon nanotubes on elastomeric substrates. *Nano Lett.* **8**, 124–130 (2008).
- Chang, L. *Foundations of MEMS* (Pearson Education, Inc., Upper Saddle River, New Jersey, 2006).
- Weaver, W., Timoshenko, S. P. & Young, D. H. *Vibration Problems in Engineering* 5th edn, Ch. 6 (Wiley Interscience, New York, 1990).

Supplementary Information accompanies this paper at www.nature.com/naturenanotechnology.

Acknowledgements

We thank Y. Yamamoto, N. Makimoto, S. Yamada and T. Kikuchi for technical assistance. Partial support by the New Energy and Industrial Technology Development Organization (NEDO) and Highly Integrated, Complex MEMS Production Technology Development Project is acknowledged.

Author contributions

Y.H. conducted and designed the experiments; T.Y. contributed to process development of planar and 3D nanotube structures; K.M. contributed to CNT wafer; D.F. contributed to CNT synthesis; R.D. contributed to process development; K.H. designed and conceived the experiments and wrote the paper.

Author information

Reprints and permission information is available online at <http://npg.nature.com/reprintsandpermissions/>. Correspondence and requests for materials should be addressed to K.H.